Integrating the Kuramoto-Sivashinsky equation in polar coordinates: Application of the distributed approximating functional approach

De S. Zhang,* Guo W. Wei,† and Donald J. Kouri‡
Department of Chemistry and Department of Physics, University of Houston, Houston, Texas 77204

David K. Hoffman§
Department of Chemistry and Ames Laboratory, Iowa State University, Ames, Iowa 50011

Michael Gorman and Antonio Palacios
Department of Physics, University of Houston, Houston, Texas 77204

Gemunu H. Gunaratne‖
Department of Physics, University of Houston, Houston, Texas 77204
and The Institute of Fundamental Studies, Kandy, Sri Lanka
(Received 19 January 1999)

An algorithm is presented to integrate nonlinear partial differential equations, which is particularly useful when accurate estimation of spatial derivatives is required. It is based on an analytic approximation method, referred to as distributed approximating functionals (DAF's), which can be used to estimate a function and a finite number of derivatives with a specified accuracy. As an application, the Kuramoto-Sivashinsky (KS) equation is integrated in polar coordinates. Its integration requires accurate estimation of spatial derivatives, particularly close to the origin. Several stationary and nonstationary solutions of the KS equation are presented, and compared with analogous states observed in the combustion front of a circular burner. A two-ring, nonuniform counter-rotating state has been obtained in a KS model simulation of such a burner.
[S1063-651X(99)02409-5]

PACS number(s): 02.70.−c, 47.54.+r

I. INTRODUCTION

Recent studies of well-controlled experimental systems and extensive use of computing have provided impetus to significant developments in the study of pattern formation. Even though the experimental systems (e.g., chemical systems [1], convecting fluids [2], flame fronts [3]) are governed by complex nonlinear spatio-temporal dynamics, qualitative aspects of pattern formation can be analyzed using simplified models of the phenomena [4]. In particular, classification of possible states of a system and determination of the interrelationships between various stationary and nonstationary patterns are amenable to such analyses. These interrelationships, though robust to some variations of the model, depend critically on the symmetries of the underlying system. Thus, it is *crucial* to retain all relevant symmetries in integrating a model system.

Cellular flame patterns stabilized on a circular porous plug burner exhibit a wide array of complex spatio-temporal states with novel features. In order to design and develop an efficient burner system, these time dependences of the flame front need to be suppressed. One of the authors [3,5–7] has carried out extensive experimental studies on a circular burner and categorized many complex states. The experiments, which are mounted in a larger combustion chamber, involve the combustion of premixed air and fuel, providing uniform conditions within the circular combustion front [3]. The temperature outside this disk is significantly lower than that of the flame front itself. For suitable control parameters, the flat uniform flame front undergoes spontaneous symmetry breaking, producing ordered patterns of brighter, hotter cells separated by darker, cooler cusps and folds. On varying control parameters, the system exhibits several types of nonstationary states including uniform rotations [3], intermittent motions [5], and chaotic dynamics [6]. Qualitative aspects of the patterns and their dynamics are believed to be related to the symmetry of the system. For example, patterns consist of ''rings'' of cells; the cells within a ring are very strongly coupled, while the rings themselves are weakly coupled to each other. For example, one ring of cells can remain stationary while a second undergoes motion that can be as simple as uniform rotation or as complex as ratcheting [5].

The bifurcations leading to and from many of these complex states have not been analyzed primarily because the principal modes are unknown. Observations of analogous states in a model system will allow the determination of the principal modes and help the development of the relevant normal form analyses. A phenomenological model for the flame front that includes a modification of the Brusselator [8] has also been used for this purpose [9–11].

The Kuramoto-Sivashinsky (KS) equation [12,13] is one of the simplest models describing the spatio-temporal evolution of a flame front [14]. It is derived by making a series of

*Electronic address: dzhang@kitten.chem.uh.edu
†Electronic address: guowei@kitten.chem.uh.edu
‡Electronic address: kouri@uh.edu
§Electronic address: hoffman@ameslab.gov
‖Electronic address: gemunu@uh.edu

simplifying assumptions on a pair of diffusion equations (for a single chemical species and temperature) coupled to fluid equations [15,16]. At low driving, the solution to the KS equation is smooth, and can exhibit spatio-temporal chaos for certain control parameters. The low-dimensional dynamics generated by the KS equation in one dimension and square domains have been the subject of intense theoretical and computational study [12–14,16–21]. Of interest to us are the structure and properties of cellular solutions of the KS equation in a circular domain.

We consider a form of the KS equation that describes the evolution of a field $u(\mathbf{x},t)$ according to

$$\frac{\partial u}{\partial t} = -\epsilon u - 2\nabla^2 u - \nabla^4 u - (\nabla u)^2 - \eta u^3, \tag{1}$$

where ϵ is a measure of the driving force and other parameters have been eliminated by suitable rescaling of the variables. The cubic term, with a small coefficient η, helps stabilize the numerical integration. The field $u(\mathbf{x},t)$ models the perturbation of a planar flame front in the direction of propagation.

The integration of the KS equation (with fixed values of ϵ and ν) is carried out in a circular domain whose radius R is used as the control parameter. Motivated by experimental conditions, we require the field to be in the trivial state [i.e., $u(\mathbf{x},t)=0$] outside this domain. In order to preserve the $O(2)$ symmetry (of the burner), it is necessary to carry out the integration of the model in plane polar coordinates (r,ϕ). The absence of periodic boundary conditions renders spectral methods unsuitable for the integration, and suggests the use of an implicit grid method. In polar coordinates, the Laplacian $\nabla^2=(\partial_{rr}+2r^{-1}\partial_r+r^{-2}\partial_{\phi\phi})$ contains a (coordinate) singularity at the origin. Even though the singularity can be avoided by partitioning each diameter into an even number of equally spaced lattice points, the presence of small denominators at grid points close to the origin makes integration of the model sensitive to the accuracy of the spatial derivatives. The nonseparable cross derivatives present in the expansion of the ∇^4 term complicate the computation further [22]. The inability of traditional methods to provide sufficient accuracy to maintain numerical stability has prevented the integration of the KS equation in polar coordinates. These problems are exacerbated in the study of nonstationary patterns.

In this paper we employ a method to obtain an analytic approximation to a function that is sampled on a discrete grid. The basic tool for discretizing the KS equation in space is an ''approximate identity kernel'' known as a ''distributed approximating functional'' (DAF). Methods to estimate the function and a finite number of derivatives to a specified accuracy *on and off* the discrete grid have been developed [23–38]. These methods are coupled with a semi-implicit algorithm to carry out our integrations.

The remainder of the paper is organized as follows. Section II gives a brief description of the DAF formalism and methods to obtain the analytic approximations. Section III describes the semi-implicit solution method and its application to discretize the KS equation. In Sec. IV, we present several stationary and nonstationary cellular states obtained by integrating the KS equation. A modal decomposition of the states based on a Fourier-Bessel expansion, and the implications of the results, are discussed in Sec. V while the concluding Sec. VI includes a brief discussion of our results.

II. DISTRIBUTED APPROXIMATING FUNCTIONALS

The theory of distributed approximating functionals (DAF's) has been extensively discussed [23–29]. It was introduced [23,24] as a means of fitting or approximating a continuous L^2 function using (possibly noisy) values known only on a discrete set of points and estimating linear transformations of the function, particularly its derivatives. The most interesting feature of a class of commonly used DAF's is the so-called ''well-tempered'' property, which distinguishes the DAF's from many other numerical approaches (e.g., basis expansions, wavelets, splines, finite differences, finite elements, etc.). There are no ''special points'' in the well-tempered DAF approximation, i.e., the DAF approximation to a function yields a similar order of accuracy for the function on or off the grid points. This is in contrast to interpolation, which yields exact results for the function on the grid points, but often at the expense of giving poor results for the function off the grid points, leading to less accurate estimation of derivatives. Another feature of the DAF is that it yields an integral representation of differential operators; i.e., it is basically an integral identity kernel. The ability of the DAF to provide a controllably accurate analytical representation of derivatives of the function on the grid points is crucial to its success in solving nonlinear partial differential equations (NPDE's). Other realizations of DAF's have been proposed [23,30,31] for different applications. We limit the discussion below to the Hermite DAF (HDAF), and for simplicity we present the discussion in one dimension. The multidimensional extensions are straightforward.

The Dirac δ function satisfies

$$f(x)=\int_{-\infty}^{\infty}\delta(x-x')f(x')dx', \tag{2}$$

$$f^{(l)}(x)=\int_{-\infty}^{\infty}\delta^{(l)}(x-x')f(x')dx', \tag{3}$$

where the superscript l denotes the lth spatial derivative. Relations (2) and (3) have no numerical utility because $\delta(x)$ is not a function in the true sense and cannot be directly approximated by quadrature. The form of the HDAF approximate identity integral kernel (or approximation to the Dirac δ function) is constructed using the Hermite polynomials H_{2n} as

$$I(x-x')=\frac{1}{\sigma}\exp(-z^2)\sum_{n=0}^{M/2}\left(-\frac{1}{4}\right)^n\frac{1}{\sqrt{2\pi}n!}H_{2n}(z), \tag{4}$$

where $z=(x-x')/\sigma\sqrt{2}$ while σ and M are the DAF parameters. The behavior of $I(x-x')$ is dominated by the Gaussian factor $\exp(-z^2)$, which serves to control the effective width of the function. In the limits of $M\to\infty$ or $\sigma\to 0$, the HDAF approaches the Dirac δ function. In analogy to properties of $\delta(x)$, the approximation to a function is given by the continuous DAF mapping

$$f(x)\approx f_{\mathrm{DAF}}(x)=\int_{-\infty}^{\infty} I(x-x')f(x')dx'. \tag{5}$$

Using the HDAF, approximations to linear transformations of the continuous function can also be performed; e.g., the derivative to order l is given by

$$f^{(l)}(x)\approx f^{(l)}_{\mathrm{DAF}}=\int_{-\infty}^{\infty} I^{(l)}(x-x')f(x')dx', \tag{6}$$

where $I^{(l)}(x-x')$ is the lth derivative of $I(x-x')$ and is given by

$$I^{(l)}(x-x')=\frac{2^{-l/2}}{\sigma^{l+1}}\exp(-z^2) \times\sum_{n=0}^{M/2}\left(-\frac{1}{4}\right)^n(-1)^l\frac{1}{\sqrt{2\pi}n!}H_{2n+l}(z). \tag{7}$$

In contrast to Eqs. (2) and (3), the HDAF approximation to the function [Eq. (5)] and its derivatives [Eq. (6)] can be discretized by quadrature (or by random sampling or Monte Carlo integration). From known values of the function on a set of discrete grid points, the HDAF approximation to the function (on or off the grid points) is given by

$$f(x)\approx f_{\mathrm{DAF}}(x)=\Delta\sum_j I(x-x_j)f(x_j), \tag{8}$$

$$f^{(l)}(x)\approx f^{(l)}_{\mathrm{DAF}}(x)=\Delta\sum_j I^{(l)}(x-x_j)f(x_j), \tag{9}$$

where Δ is the uniform grid spacing. Significant contributions to the summation come only from grid values at points close to x.

With a suitable choice of the DAF parameters M and σ, it is possible to estimate the function and a finite number of spatial derivatives to a desired accuracy [24,25]. This important feature makes the DAF's a powerful computational tool for solving linear and nonlinear PDE's, such as Burgers' equation in one and two dimensions [32,33], the linear [34] and nonlinear [35] Fokker-Planck equation in statistical mechanics, the Sine-Gordon equation [36] (for which previous methods produced ''artifical,'' numerically induced chaos because of insufficient accuracy in approximating derivatives), the KdV equation [37] describing the dynamics of solitons, and the Navier-Stokes equation [38] in fluid dynamics.

III. APPLICATION OF THE DISTRIBUTED APPROXIMATING FUNCTIONAL TO THE IMPLICIT METHOD

Two numerical approaches that have been used to perform the time integration are the explicit method and the implicit method [39]. In some cases, the DAF-based explicit method (e.g., Taylor expansion method or the Runge-Kutta method) is robust, efficient, and gives accurate results. However, like most explicit methods, in order to maintain numerical stability, the DAF-based explicit method requires a time step Δt that approximately scales linearly with the grid spacing. Thus, the smaller the grid spacing, the smaller the time step required to maintain stability. In contrast, implicit methods permit larger time steps and are typically more stable than explicit methods. Computationally, implicit methods require the solution of simultaneous linear algebraic equations, which involves substantial CPU time when high accuracy of spatial derivatives is required. The integration of the KS equation is done semi-implicitly [39] because stability is crucial, regardless of the CPU cost. In order to avoid the need to solve nonlinear equations, each nonlinear term is expanded up to first order in $\delta u=u_{mn}(t+\delta t)-u_{mn}(t)$, thus linearizing the equations in $u_{mn}(t+\delta t)$. The fields $u_{mn}(t)$, $u_{mn}(t+\delta t)$, and their derivatives are evaluated according to Eq. (9). Given $u_{mn}(t)$, inverting the set of N_rN_ϕ linear equations gives the new grid values $u_{mn}(t+\delta t)$ of the field, where N_r is the number of radial and N_ϕ is the number of angular grid points.

Consider a partial differential equation (PDE) describing an initial value problem

$$u_t\equiv\frac{\partial u}{\partial t}=F(\vec{\mathbf{r}},t,u,\nabla u,\cdots) \tag{10}$$

subject to the initial condition $u(\vec{r},0)$. Here, F is a functional of u and its derivatives; e.g., the right-hand side of Eq. (1). The DAF-based implicit method converts the task of solving the PDE into one of solving a set of simultaneous linear algebraic equations

$$\mathbf{A}(t)\mathbf{u}(t+\Delta t)=\mathbf{B}(t), \tag{11}$$

with $\mathbf{A}(t)$ being an $N\times N$ matrix (N being the total number of grid points). The quantity $\mathbf{u}(t+\Delta t)$ is an N-dimensional column vector solution of the discretized Eq. (10) at time $t+\Delta t$ and $\mathbf{B}(t)$ is an N-dimensional column vector inhomogeneity. We outline the computation of $\mathbf{A}(t)$ and $\mathbf{B}(t)$.

The left side of Eq. (10) is approximated using

$$\frac{\partial u}{\partial t}\approx\frac{u(t+\Delta t)-u(t)}{\Delta t}. \tag{12}$$

Notice that it is usually more accurate to interpret the difference approximation of the derivative to be midway between t and $t+\Delta t$; i.e., at $t+\frac{1}{2}\Delta t$. This suggests the approximation of u on the right side of Eq. (10) by the average of $u(t)$ and $u(t+\Delta t)$; i.e., $u\approx[u(t)+u(t+\Delta t)]/2$. We thus obtain

$$\frac{u(t+\Delta t)-u(t)}{\Delta t}=F\left(\mathbf{x},t,\frac{u(t)+u(t+\Delta t)}{2}, \times\frac{\nabla u(t)+\nabla u(t+\Delta t)}{2},\ldots\right). \tag{13}$$

When F includes nonlinear terms, we write $u(t+\Delta t)=u(t)+\delta u$ and expand F to linear order in δu. For example,

$$\left[\frac{u(t)+u(t+\Delta t)}{2}\right]^n\approx\left(1-\frac{n}{2}\right)u(t)^n+\frac{n}{2}u(t)^{n-1}u(t+\Delta t), \tag{14}$$

$$\left[\frac{u_x(t)+u_x(t+\Delta t)}{2}\right]^n \approx \left(1-\frac{n}{2}\right)u_x(t)^n + \frac{n}{2}u_x(t)^{n-1} \times u_x(t+\Delta t). \quad (15)$$

An accurate estimation of F requires a choice of δt, which gives a suitably small value for δu. Substituting these expressions into Eq. (13), and using the HDAF to represent derivatives, we obtain the set of linear algebraic equations of $u(t+\Delta t)$ which define the matrix **A** and **B** in Eq. (11).

With $u=u(t)$ and $u'=u(t+\Delta t)$, the KS equation in polar coordinates reads

$$\begin{aligned}
&\tfrac{1}{2}u'_{rrrr}+\frac{1}{r}u'_{rrr}+\tfrac{1}{2}\left(2-\frac{1}{r^2}\right)u'_{rr}+\frac{1}{2}\left(\frac{1}{r^3}+\frac{2}{r}\right)u'_r+u_ru'_r \\
&\quad+\frac{1}{2r^4}u'_{\phi\phi\phi\phi}+\left(\frac{2}{r^4}+\frac{1}{r^2}\right)u'_{\phi\phi}+\frac{1}{r^2}u_\phi u'_\phi+\frac{1}{r^2}u'_{rr\phi\phi} \\
&\quad-\frac{1}{r^3}u'_{r\phi\phi}+\left(\frac{1}{\Delta t}+\frac{\epsilon}{2}+\frac{3}{2}\eta u^2\right)u' \\
&=-\tfrac{1}{2}u_{rrrr}-\frac{1}{r}u_{rrr}-\frac{1}{2}\left(2-\frac{1}{r^2}\right)u_{rr} \\
&\quad-\frac{1}{2}\left(\frac{1}{r^3}+\frac{2}{r}\right)u_r-\frac{1}{2r^4}u_{\phi\phi\phi\phi} \\
&\quad-\left(\frac{2}{r^4}+\frac{1}{r^2}\right)u_{\phi\phi}-\frac{1}{r^2}u_{rr\phi\phi}+\frac{1}{r^3}u_{r\phi\phi} \\
&\quad+\left(\frac{1}{\Delta t}-\frac{\epsilon}{2}\right)u+\tfrac{1}{2}\eta u^3. \quad (16)
\end{aligned}$$

The right side of the expression can be evaluated from the field $u(\mathbf{x},t)$ while the left side includes the (unknown) vector $u'=u(t+\Delta t)$. By using the HDAF to approximate the derivatives on both sides, we finally obtain the matrix **A** and vector **B** in Eq. (11). The partial derivatives with respect to one spatial variable (r or ϕ) are obtained with the other variable fixed, using Eq. (9). The mixed partial derivatives are computed using

$$\frac{\partial^{l+k}u(r,\phi)}{\partial r^l\partial\phi^k}=\Delta_r\Delta_\phi\sum_i\sum_j I_r^{(l)}(r-r_i)I_\phi^{(k)}(\phi-\phi_j)u(r_i,\phi_j), \quad (17)$$

where Δ_r and Δ_ϕ are the uniform grid spacing and I_r and I_ϕ are the continuous HDAF's in r and ϕ coordinates. We note that Eq. (17) satisfies the fundamental symmetry of mixed partial derivatives,

$$\frac{\partial^{l+k}u(r,\phi)}{\partial r^l\partial\phi^k}\equiv\frac{\partial^{l+k}u(r,\phi)}{\partial\phi^k\partial r^l}. \quad (18)$$

IV. MODAL DECOMPOSITION

The mechanisms generating a given cellular state of the KS equation, and the nature of its instabilities, can be deduced by using the normal form theory [40]. Moreover, such aspects of pattern formation are expected to be model independent, and hence conclusions based on the KS equation are likely to apply to cellular states of the flame front. The derivation of the normal form theory appropriate to a given state requires a modal decomposition to a basis that reflects the symmetries underlying the physical system. In particular, a smooth field $u(r,\phi,t)$, which vanishes on the boundary of a circular domain of radius R, can be expanded in a Fourier-Bessel series as

$$u(r,\phi,t)=\sum_{n,m} z_{nm}(t)\Psi_{nm}(r,\phi)+\text{c.c.}, \quad (19)$$

where $\Psi_{nm}(r,\phi)=J_n(\alpha_{nm}r/R)e^{in\phi}$ ($m\geqslant 0$ and $n>0$) and c.c. denotes the complex conjugate [41]. Here $J_n(r)$ is the nth-order Bessel function of the first kind and α_{nm} is its mth nontrivial zero. The z_{nm} are complex coefficients, save for z_{0m}, which are real. The orthonormality and completeness of $\{\Psi_{nm}: n\geqslant 0,\ m\geqslant 1\}$ imply that

$$z_{nm}(t)=\beta\int_0^{2\pi}\int_0^R ru(r,\phi,t)\overline{\Psi}_{nm}(r,\phi)\,d\phi\,dr, \quad (20)$$

where $\beta=(1-\delta_{n0}/2)/\pi R^2J_{n+1}^2(\alpha_{nm})$. Notice that the Fourier-Bessel function Ψ_{nm} is an eigenfunction of $\boldsymbol{\nabla}^2$ with eigenvalue $k_{nm}\equiv\alpha_{nm}^2/R^2$; thus the linear stability analysis of the trivial state $u(\mathbf{x},t)=0$ of Eq. (1) is considerably simplified [10]. By examining the magnitude and the phase of the expansion coefficients z_{nm}, we can determine the principal modes that play important roles in determining the geometry and dynamics of the field $u(r,\phi,t)$. Furthermore, once the principal modes for a given state have been determined, the spatio-temporal evolution of the field can be reduced to a set of ordinary differential equations that govern the dynamics of the z_{nm}'s.

V. EXAMPLES

In order to avoid having a grid point at the origin (which would lead to divergences due to the singularity of $\boldsymbol{\nabla}^2$ in polar coordinates), each diameter is partitioned into the $2N_r$ lattice points $(r_m,\phi_n)=((m+1/2)\Delta_r,n\Delta_\phi)$, where the lattice spacings are $\Delta_r=R/(N_r+1/2)$ and $\Delta_\phi=2\pi/N_\phi$. Here N_ϕ is the number of evenly spaced radial lines indexed by azimuthal angle.

The calculations reported here were carried out using grid parameters $N_r=32$ and $N_\phi=64$, and with $M=54$ and $\sigma_r/\Delta_r=\sigma_\phi/\Delta_\phi=2.36$, which are ''well-tempered'' DAF parameters known to provide sufficient accuracy for evaluating the required spatial derivatives [24,25]. The initial state was chosen such that its amplitude was a fraction of that of the final state. We now present several examples of stationary and nonstationary solutions observed in the integration of

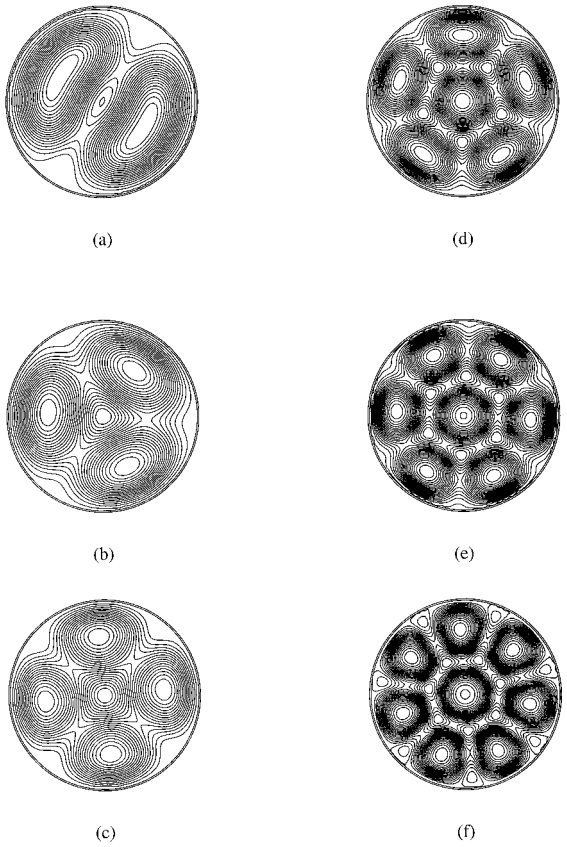

FIG. 1. Several stationary cellular solutions generated in the KS equation [Eq. (1)]. $\epsilon = 0.7$ and $\eta = 0.03$ are fixed while the radius R of the domain is used as the control parameter. Structures shown are generated with (a) $R = 5.95$, (b) $R = 6.5$, (c) $R = 7.5$, (d) $R = 9.5$, (e) $R = 10.0$, and (f) $R = 11.6$. Note that individual cells of each state are chirally symmetric.

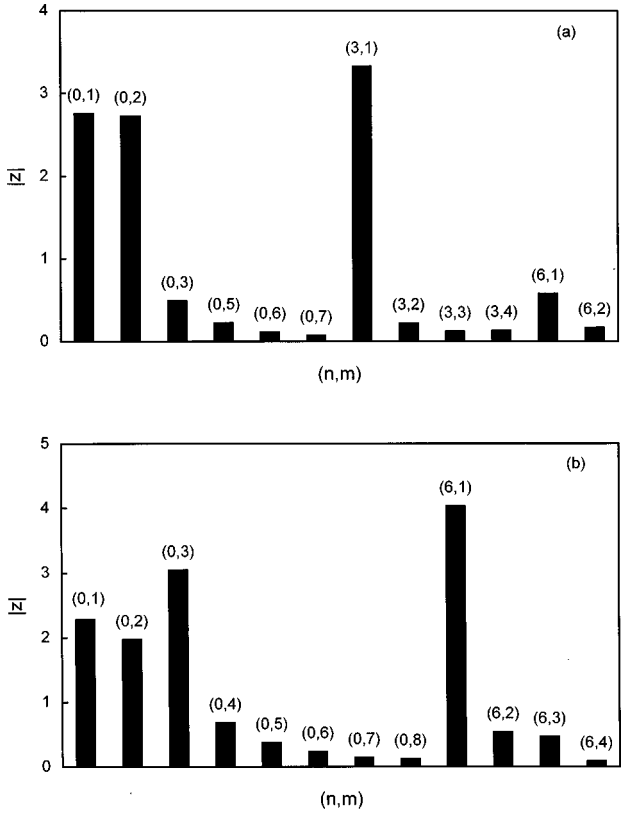

FIG. 3. Magnitudes of the relevant Fourier-Bessel coefficients of the stationary states shown in Figs. 1(b) and 1(e). The Fourier-Bessel coefficients z_{nm} of each stationary state have the same phase, implying the observed chiral symmetry of the cells.

the KS equation on the circular domain. The results presented here are obtained by integrating the KS equation with fixed values of ϵ $(=0.7)$ and ν $(=0.03)$. The radius R of the circular domain is used as the control parameter.

Figure 1 shows six stationary cellular states; patterns shown in Figs. 1(a), 1(b), and 1(c) have a single ring of cells, while those of Figs. 1(d), 1(e), and 1(f) have two rings of cells. Figure 2 shows the variations of the intensity for two of these stationary cellular states. The cells in these stationary states have ''chiral symmetry''; i.e., the cells are symmetric under reflection about a suitable axis. Each ring of the patterns exhibits a dihedral symmetry D_n, n being the number of cells in the ring. Furthermore, the number of cells contained in a ring increases with its ''radius.''

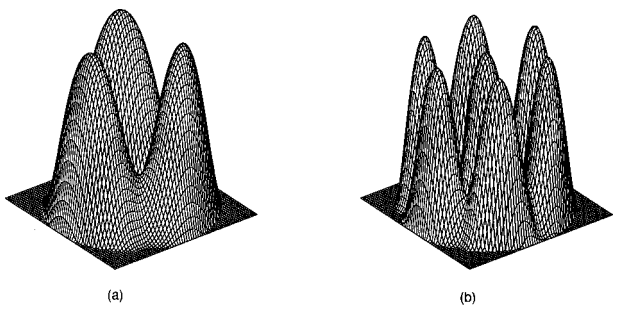

FIG. 2. Intensities of (a) pattern with three cells [Fig. 1(b)] and (b) two rings of one and six cells [Fig. 1(e)].

Results from the Fourier-Bessel decomposition of these two states are shown in Fig. 3. The principal modes of the stationary state with a single ring of three cells [Fig. 3(a)] are Ψ_{01}, Ψ_{02}, and Ψ_{31}. The first two modes make circularly symmetric contributions and the last provides the observed threefold symmetry of the pattern. In addition, ''harmonics'' Ψ_{6m} of smaller amplitude, whose presence is a consequence of the nonlinear gradient terms in the KS equation [10], are observed. Each Fourier-Bessel coefficient z_{3m} and z_{6m} has the same phase, resulting in the observed chiral symmetry of the cells. The Fourier-Bessel decomposition of the two-ring state, shown in Fig. 2(b), is presented in Fig. 3(b). The principal modes of the state are of the form Ψ_{0m} and Ψ_{6m}, which represent the inner ring (of a single cell) and the outer ring (of six cells). As before, the phases of all z_{6m}'s are the same, leading to chiral symmetry of the cells. A normal form analysis of this two-ring state will involve the interaction of two modes with D_0 and D_6 symmetries [10].

We next present two non-stationary solutions of the model and conclusions that follow from their Fourier-Bessel decompositions. Figure 4 shows several snapshots during the formation of a uniformly rotating two-cell state from a random initial state. Unlike in stationary states, the cells of the rotating ring are not chirally symmetric. The sense of the geometrical asymmetry depends on the initial state and is

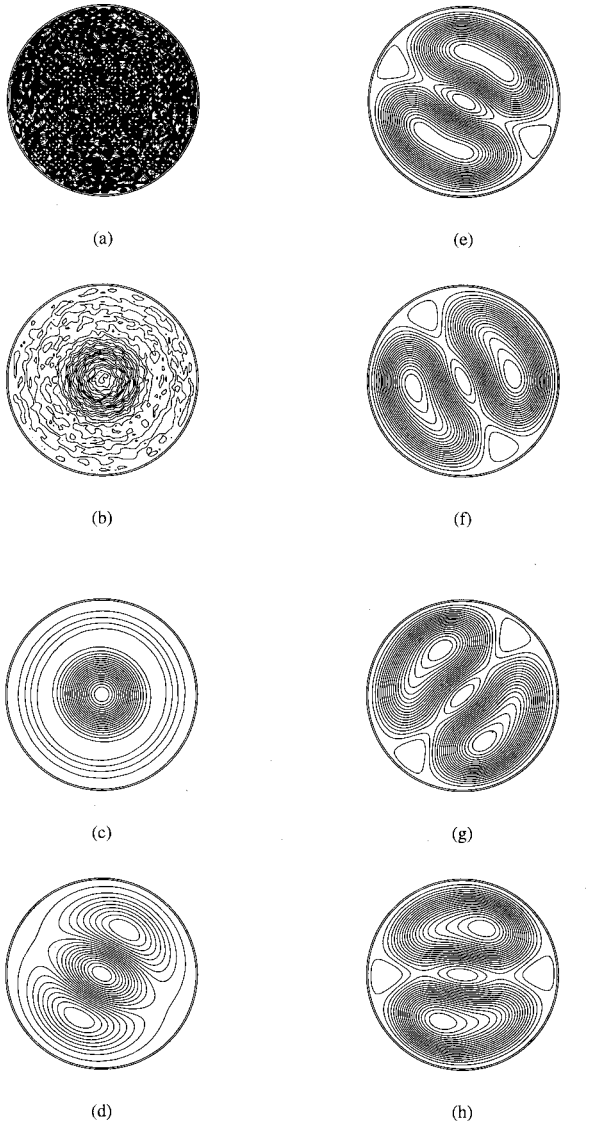

FIG. 4. Snapshots from the evolution of a random initial state under the KS equation at a radius $R=6.2$ where a uniformly rotating two-cell state is observed. The sense of the geometrical asymmetry depends on the initial state. The patterns are shown at times (in terms of arbitrary units) (a) $t=0$, (b) $t=20$, (c) $t=50$, (d) $t=80$, (e) $t=150$, (f) $t=190$, (g) $t=250$, and (h) $t=300$.

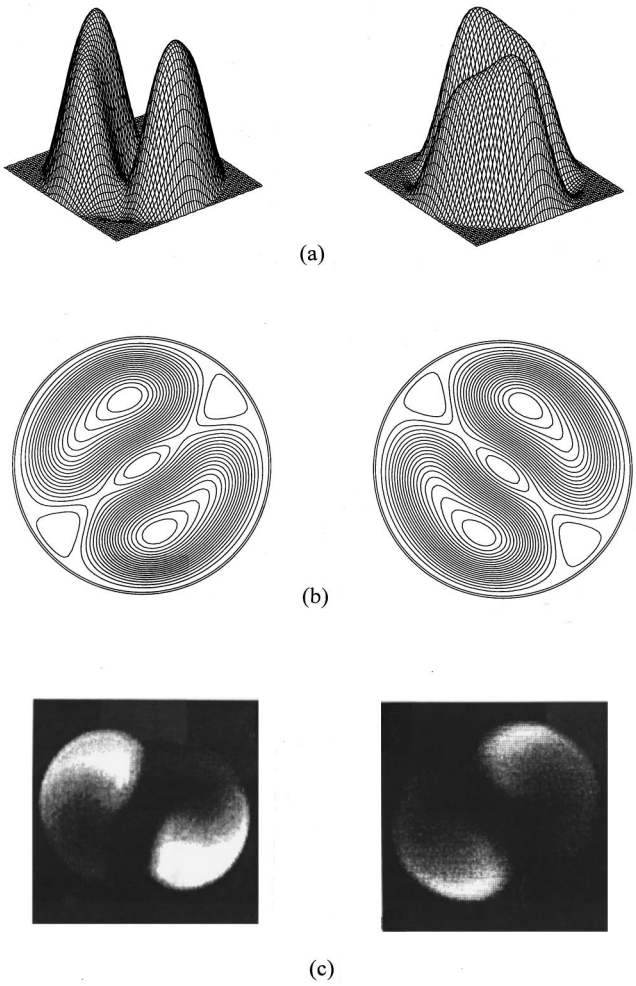

FIG. 5. The (a) intensity and (b) contours of clockwise (left) and counterclockwise (right) rotating two-cell solutions of the KS equation. (c) shows analogous states observed in the experimental flame front. The sense of geometrical asymmetry of a cell is related to the direction of motion of the ring which contains the cell.

related to the direction of motion of the cells. This is elaborated in Fig. 5 and compared with corresponding states from the experimental flame front.

The magnitudes of the Fourier-Bessel coefficients (Fig. 6) show that the principal modes are of the type Ψ_{0m}, Ψ_{2m}, and Ψ_{4m}. The magnitudes of z_{21} and z_{41} are fixed in time, while their phases increase uniformly (Fig. 7). Furthermore, there is a nonzero phase difference between the two modes, which results in the chiral asymmetry of the cells. Normal form analysis of the coupling of Ψ_{21} and Ψ_{41} reveals that the motion of the cells (i.e., the increase of the phases of the z_{mn}'s) is a consequence of the asymmetry of the cells (i.e., phase difference between the coefficients) [10].

Figure 8(a) shows a cellular state that exhibits more complex dynamics. The outer ring of eight cells rotates clockwise, while the inner ring of two cells rotates in a counterclockwise direction with a larger angular speed. Figure 8(b) shows a snapshot of an analogous cellular state from the flame front with counter-rotating rings of cells. The number of cells in the outer ring is different (six) for the experimen-

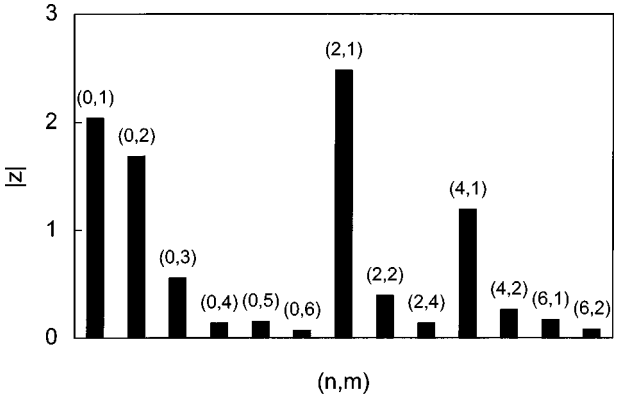

FIG. 6. Magnitudes of the relevant Fourier-Bessel coefficients of a uniformly rotating two-cell state. The magnitudes of the z_{nm}'s remain fixed in time. The phases of z_{21} and z_{41} are different, leading to the observed chiral asymmetry of the cells.

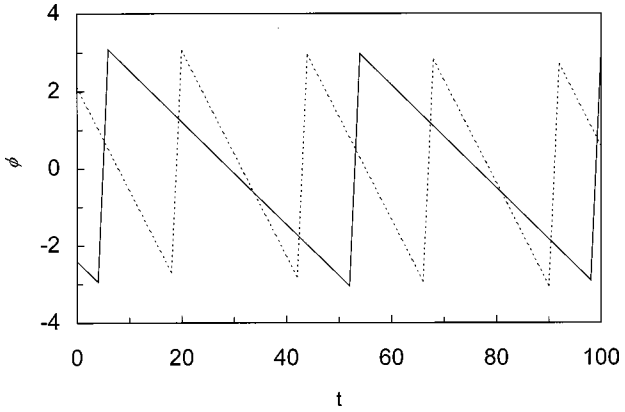

FIG. 7. Time evolution of the phase of the Fourier-Bessel coefficients z_{21} (solid line) and z_{11} (dashed line). The angular velocity of the ring is seen to be constant.

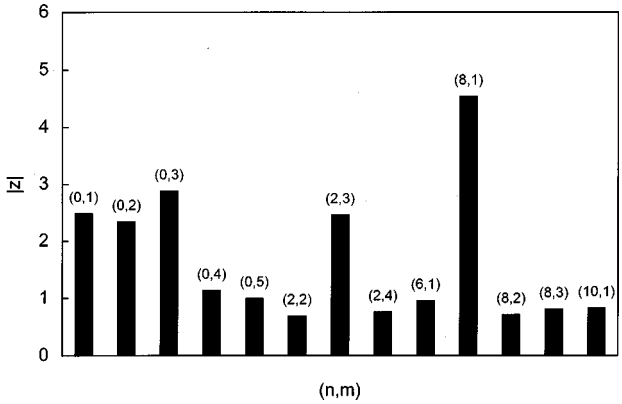

FIG. 9. Magnitudes of the relevant Fourier-Bessel coefficients for the cellular state with two counter-rotating rings. These magnitudes vary periodically in time, resulting in periodic modulations of the cell shape.

tal state. The stability of such complex states depends sensitively on the control parameters chosen for the model. With the approximations that have gone into the derivation of the KS equation and our arbitrary choice of ϵ and ν, we do not expect, necessarily, to obtain the exact states observed in the experiment. However, that we are able to obtain patterns with the similar qualitative features is significant; they can be used to develop a modal decomposition of these states and to develop an understanding of the mechanisms generating them.

As seen from Fig. 9, the principal modes of the counter-rotating state are Ψ_{23} and Ψ_{81}, which correspond to the two rings of cells. Smaller components (not shown) of Ψ_{41} and $\Psi_{16,1}$ which are not in phase with the principal modes produce the asymmetry of the cells and their motion. Fourier-Bessel analysis of the state reveals that the rotation of the cells is periodic rather that uniform (see Fig. 10). It can also be checked that the magnitudes of the Fourier-Bessel coefficients, and hence the shape of the cells, are periodic in time. It would be virtually impossible to glean such information by direct observation of the spatio-temporal dynamics. To the best of our knowledge, complex, nonuniform motion of this type has never been observed before in model systems with circular symmetry.

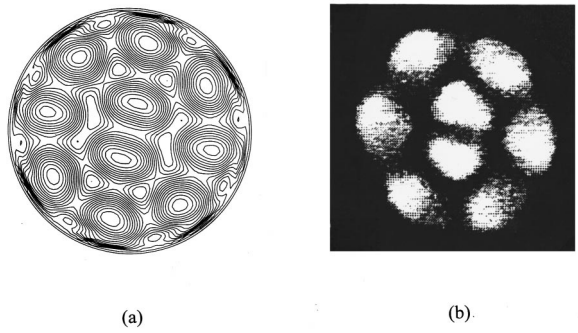

FIG. 8. (a) A solution of the KS equation with two counter-rotating rings of cells. The inner ring of two cells moves counter-clockwise while the outer ring moves clockwise with a smaller angular velocity. This solution is generated with $\epsilon=0.7$, $\eta=0.02$, and $R=12.0$. (b) An analogous state on the flame front.

VI. CONCLUSIONS AND DISCUSSION

We have carried out a successful numerical integration of the Kuramoto-Sivashinsky equation in a circular domain. This was made possible by the use of distributed approximating functionals, which allowed accurate estimations of the

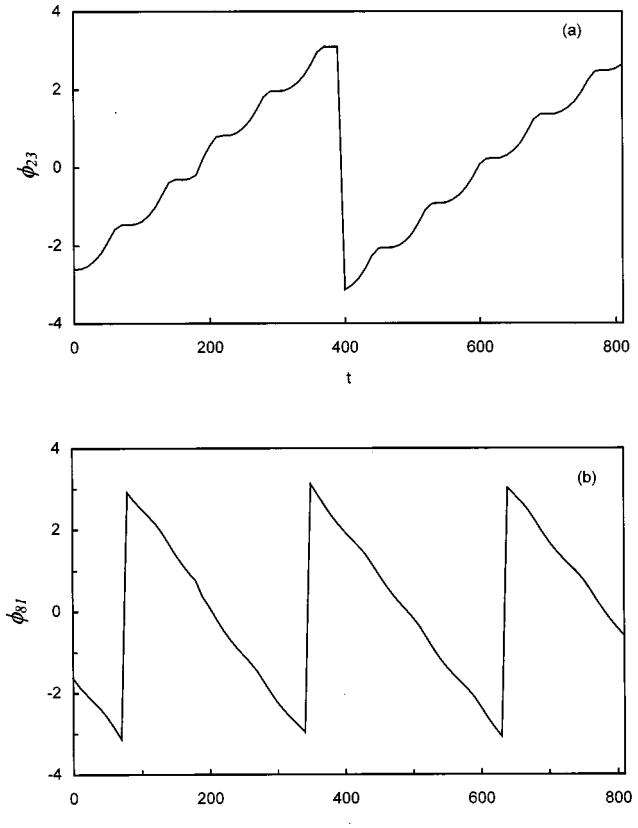

FIG. 10. Time evolution of the phases of (a) z_{23} and (b) z_{81} confirm the sense of rotation of each ring of Fig. 8(a) and indicate that the angular velocity of each ring is periodic in time. The periodicity of the angular velocity is identical to that of the modulations in the cell shape.

spatial derivatives from values of the field given on a polar grid. A semi-implicit method, complemented by the use of DAF's introduced here, provided the ability to take large time steps in the computations. The methods discussed can be used to integrate other nonlinear partial differential equations and are expected to be most useful when accurate estimations of spatial derivatives are required.

We presented several stationary and nonstationary solutions of the KS equation and carried out a modal decomposition using the Fourier-Bessel functions. The decomposition helps identify the principal modes that are contained in each state and suggest methods to recognize the onset of such states. The normal form analysis appropriate to study the coupling of these modes provides information about the instabilities of each state. An analysis of the Fourier-Bessel coefficients of the states confirmed that cells in stationary rings are chirally symmetric, while those in rotating rings are not. The analysis also allows us to deduce the nature of rotation of the rings.

ACKNOWLEDGMENTS

Informative discussions with B. Matkowsky, I. Melbourne, and M. Golubitsky are gratefully acknowledged. This research was partially funded by the National Science Foundation (G.W.W. and D.J.K.), R. A. Welch Foundation (D.S.Z. and D.J.K.), the Department of Energy (D.K.H. and the Ames Laboratory, Iowa State University), Office of Naval Research (M.G. and G.H.G.), and the Energy Laboratory of the University of Houston (D.J.K., M.G., and G.H.G.).

[1] Q. Ouyang and H. L. Swinney, Nature (London) **352**, 610 (1991).
[2] M. S. Heutmaker and J. P. Gollub, Phys. Rev. A **35**, 242 (1987).
[3] M. Gorman, F. Hamill, M. el-Hamdi, and K. Robbins, Combust. Sci. Technol. **98**, 25 (1994).
[4] M. C. Cross and P. C. Hohenberg, Rev. Mod. Phys. **65**, 851 (1993).
[5] M. Gorman, M. el-Hamdi, and K. Robbins, Combust. Sci. Technol. **98**, 71 (1994).
[6] M. Gorman, M. el-Hamdi, and K. Robbins, Combust. Sci. Technol. **98**, 79 (1994).
[7] M. Gorman, B. Pearson, M. el-Hamdi, and K. A. Robbins, Phys. Rev. Lett. **76**, 228 (1996).
[8] I. Prigogine and R. Lefever, in *Membranes, Dissipative Structures, and Evolution*, edited by G. Nicholis and R. Lefever (Wiley, New York, 1974).
[9] G. H. Gunaratne, M. el-Hamdi, M. Gorman, and K. A. Robbins, Mod. Phys. Lett. B **10**, 1379 (1996).
[10] A. Palacios, G. H. Gunaratne, M. Gorman, and K. A. Robbins, Chaos **7**, 463 (1997).
[11] A. Palacios, G. H. Gunaratne, M. Gorman, and K. A. Robbins, Phys. Rev. E **57**, 5958 (1998).
[12] G. I. Sivashinsky, Acta Astron. **4**, 1177 (1977).
[13] Y. Kuramoto, Prog. Theor. Phys. Suppl. **64**, 346 (1978).
[14] U. Frisch, Z. S. She, and O. Thual, J. Fluid Mech. **168**, 221 (1986).
[15] M. L. Frankel and G. I. Sivashnsky, Physica D **30**, 28 (1988).
[16] S. B. Margolis and B. J. Matkowsky, Combust. Sci. Technol. **34**, 45 (1983).
[17] J. M. Hyman and B. Nicolaenko, Physica D **18**, 113 (1986).
[18] H. S. Brown, I. G. Kevrekidis, A. Oron, and P. Rosenau, Phys. Lett. A **163**, 299 (1992).
[19] G. I. Sivashinsky, Combust. Sci. Technol. **15**, 137 (1977).
[20] M. S. Jolly, I. G. Kevrekidis, and E. S. Titi, Physica D **44**, 38 (1990).
[21] K. R. Elder, J. D. Gunton, and N. Goldenfeld, Phys. Rev. E **56**, 1631 (1997).
[22] To study a particular structure, one may use a suitable orthonormal expansion (in this case the Fourier-Bessel expansion) and rewrite Eq. (1) in terms of these modes. However, such an approach is unsuitable for a comprehensive analysis of the many different stationary and nonstationary cellular patterns. In addition, the presence of the $(\nabla u)^2$ term leads to the necessity of retaining a large number of FB modes [10].
[23] D. K. Hoffman, N. Nayar, O. A. Sharafeddin, and D. J. Kouri, J. Phys. Chem. **95**, 8299 (1991).
[24] D. K. Hoffman and D. J. Kouri, J. Phys. Chem. **96**, 1179 (1992).
[25] D. J. Kouri and D. K. Hoffman, J. Phys. Chem. **95**, 9631 (1992).
[26] D. J. Kouri, W. Zhu, X. Ma, B. M. Pettitt, and D. K. Hoffman, J. Phys. Chem. **96**, 9622 (1992).
[27] D. K. Hoffman, M. Arnold, and D. J. Kouri, J. Phys. Chem. **96**, 6539 (1992).
[28] D. K. Hoffman, M. Arnold, and D. J. Kouri, J. Phys. Chem. **97**, 1110 (1993).
[29] D. K. Hoffman, T. L. Marchioro, M. Arnold, Y. Huang, W. Zhu, and D. J. Kouri, J. Math. Chem. **20**, 117 (1996).
[30] G. W. Wei, D. S. Zhang, D. J. Kouri, and D. K. Hoffman, Phys. Rev. Lett. **79**, 775 (1997).
[31] D. K. Hoffman, G. W. Wei, D. S. Zhang, and D. J. Kouri, Chem. Phys. Lett. **287**, 119 (1998).
[32] D. S. Zhang, G. W. Wei, D. J. Kouri, and D. K. Hoffman, Phys. Fluids **9**, 1853 (1997).
[33] G. W. Wei, D. S. Zhang, D. J. Kouri, and D. K. Hoffman, Comput. Phys. Commun. **111**, 93 (1998).
[34] G. W. Wei, D. S. Zhang, D. J. Kouri, and D. K. Hoffman, J. Chem. Phys. **107**, 3239 (1997).
[35] D. S. Zhang, G. W. Wei, D. J. Kouri, and D. K. Hoffman, Phys. Rev. E **56**, 1197 (1997).
[36] D. J. Kouri, D. S. Zhang, G. W. Wei, T. Konshak, and D. K. Hoffman, Phys. Rev. E **59**, 1274 (1999).
[37] G. W. Wei, D. S. Zhang, D. J. Kouri, and D. K. Hoffman, Comput. Phys. Commun. **111**, 87 (1998).
[38] G. W. Wei, D. S. Zhang, S. Althorpe, D. J. Kouri, and D. K. Hoffman, Comput. Phys. Commun. **115**, 18 (1998).
[39] W. H. Press, B. P. Flannery, S. A. Teukolsky, and W. T. Vettering, *Numerical Recipes—The Art of Scientific Computing* (Cambridge University Press, Cambridge, 1988).
[40] M. Golubitsky, I. Stewart, and D. G. Schaeffer, *Singularities and Groups in Bifurcation Theory, Vol. 2* (Springer-Verlag, New York, 1988).
[41] G. Watson, *A Treatise on the Theory of Bessel Functions* (Cambridge University Press, Cambridge, England, 1962).